Combustion and Flame 161 (2014) 311–321

Contents lists available at ScienceDirect

Combustion and Flame

journal homepage: www.elsevier.com/locate/combustflame

Aluminum agglomeration reduction in a composite propellant using tailored Al/PTFE particles

Travis R. Sippel [1,*], Steven F. Son, Lori J. Groven [2]

School of Mechanical Engineering, Purdue University, 500 Allison Road, Chaffee Hall, West Lafayette, IN 47907, USA

ARTICLE INFO

Article history:
Received 19 May 2013
Received in revised form 24 July 2013
Accepted 13 August 2013
Available online 8 September 2013

Keywords:
Aluminum
Agglomeration
Solid propellant
Combustion
Mechanical activation
Polytetrafluoroethylene

ABSTRACT

In solid propellants, aluminum is widely used to improve performance, yet theoretical specific impulse is still not achieved largely because of two-phase flow losses. Losses could be reduced if aluminum particles quickly ignited, more gaseous products were produced and if upon combustion, aluminum particle breakup occurred. To explore this, tailored, fuel-rich, mechanically activated composite particles (aluminum/polytetrafluoroethylene, Al/PTFE 90/10 and 70/30 wt.%) are considered as replacements for reference aluminum powders (spherical, flake, or nanoscale) in a composite solid propellant. The effects on burning rate, pressure dependence, and aluminum ignition, combustion, and agglomeration are quantified. Using microscopic imaging, it is observed that tailored particles promptly ignite at the burning surface and appear to breakup into smaller particles, which can increase the heat feedback to the burning surface. Replacement of spherical aluminum with Al/PTFE 90/10 wt.% does not significantly affect propellant burning rate. However, Al/PTFE 70/30 wt.% increases the pressure exponent from 0.36 to 0.58, which results in a 50% increase in propellant burning rate at 13.8 MPa. This increased pressure sensitivity is consistent with more kinetically controlled combustion that occurs from smaller burning metal particles near the surface. Combustion products were quench collected using a new, liquid-free technique at 2.1 and 6.9 MPa and were measured. Both Al/PTFE 90/10 and 70/30 wt.% composite particles reduce the coarse product fraction and diameter. The most significant reduction occurs from 70/30 wt.% particle use, where average coarse product diameter is 25 μm, which is smaller than the original, average particle size and is also smaller than the 76 μm products collected from reference spherical aluminized propellant. This is a 66% decrease in agglomerate diameter or a 96% decrease in volume compared to agglomerates formed from reference spherical aluminum. Smaller diameter condensed phase products and more gaseous products will likely decrease two-phase flow loss and reduce slag accumulation.

1. Introduction

Aluminum is ubiquitous as an ingredient in propellants, explosives, and pyrotechnics and is typically used to improve performance. For example, the use of aluminum in composite solid propellants can improve specific impulse (Isp) performance by as much as 15% [1]. This performance increase follows from an increase in flame temperature and a decrease in gaseous product molecular weight (a shift from CO_2 and H_2O to CO and H_2 in propellant exhaust products). However, non-equilibrium between gas and condensed phases leads to significant losses that can reduce performance from theoretical levels by as much as 10% [1,2]. This occurs in part because relatively large product agglomerates form as a result of aluminum particles melting and coalescing prior to ignition. As these large agglomerates flow through a motor, they slow the velocity of surrounding gaseous products and fail to fully transfer their thermal energy to the flow, resulting in what is termed two-phase flow losses. Theoretically, these losses could be reduced if aluminum particles were tailored to quickly ignite at the surface, produced more gaseous products, and dispersed into smaller particles.

In addition to reducing two-phase flow losses, smaller burning particles could have other desirable effects. For example, nanoscale aluminum (nAl) particles have lower ignition temperatures [3] as well as shorter burning times [3,4]. Shorter burning times could increase heat feedback to the propellant surface. The use of smaller aluminum also may result in kinetically rather than diffusionally limited metal combustion [3,5], which in a propellant can increase the burning rate pressure dependence [6]. This might be useful for some applications, but could increase motor instability.

* Corresponding author. Fax: +1 (515) 294 3261.
E-mail address: travis.sippel@gmail.com (T.R. Sippel).
[1] Department of Mechanical Engineering, Iowa State University, 2090 Black Engineering Bldg., Ames, IA 50010.
[2] Chemical and Biological Engineering, South Dakota School of Mines, 501 East St. Joseph Street, Rapid City, SD 57701.

0010-2180/$ - see front matter © 2013 The Combustion Institute. Published by Elsevier Inc. All rights reserved.
http://dx.doi.org/10.1016/j.combustflame.2013.08.009

Despite the potential benefits, replacement of micron scale aluminum with nanoaluminum in propellants can result in a number of undesirable effects. For example, though nanoaluminum produces smaller agglomerates than micron scale aluminum [7–9], agglomeration is still prevalent. This is due to the propensity of nanoaluminum to aggregate, sinter, and coalesce due to either solid state diffusion or viscous flow [10]. For example, using 50–240 nm aluminum results in average agglomerate sizes ranging from 2 to 20 μm [7–9]. Replacement of micron scale aluminum with nanoaluminum also decreases propellant specific impulse, as nAl can contain ~10 to 25 wt.% aluminum oxide [11] and can result in poor propellant aging [12]. Additionally, the high specific surface area of nAl (~10 to 50 m^2/g) can result in high uncured propellant viscosity [13] and poor mechanical strength [14], which together can decrease propellant density, produce erratic combustion, or even motor failure. As a consequence, nanoaluminum is not currently used in fielded solid propellants.

In order to avoid problems associated with the high specific surface area of nAl, recent efforts have focused on altering agglomeration and ignition of micron scale aluminum using metallic [15–17] or polymeric [16,18] coatings. The use of coatings aims to prevent agglomeration by reducing the residence time of molten aluminum particles at the surface. This is achieved by reaction of the coating material with underlying aluminum cores at temperatures below the aluminum melting temperature. Particularly, nickel coated aluminum has received significant attention because solid-state nickel-aluminum reactions can occur [19]. In comparison to similarly sized aluminum, nickel coated aluminum can decrease agglomerate diameter by 50%, but agglomerates (~104 μm) are still about five times larger than starting particle sizes (~22 μm) [20]. Exothermic reactions of fluorocarbons with aluminum are also possible below the aluminum boiling temperature [21,22] and although reduced agglomeration has been reported using fluorinated coatings (polymethylfluoroacrylate or fluorocarbon chlorosilanes) [16,18], agglomerates were between one and two orders of magnitude larger than initial aluminum particle sizes.

In addition to exterior particle coatings, aluminum particles that contain inclusions of dissimilar materials are also of interest to reduce agglomeration. Use of composite particles in propellants has been suggested by others [23] and some initial work in this area [24] used modified aluminum particles containing significant nickel inclusion material (69 wt.%), which prohibitively reduced the theoretical specific impulse. In that work, partial replacement of ~40 μm aluminum with similarly sized mechanically activated aluminum/nickel composite particles resulted in a decrease in average agglomerate size from 235 to 90 μm. Particles containing lower levels of inclusion (10 at.% of nickel, iron, or zinc [25]; 10–20 wt.% inclusion of iodine, paraffin, or low density polyethylene [26,27]) have also been developed that may have a less detrimental effect on theoretical specific impulse. However, these particles have not been tested in propellants. These low level inclusion modified particles have decreased ignition temperatures but theoretically result in formation of additional condensed phase products or are not reactive with aluminum. In order to obtain aluminum ignition enhancement and also reduce two-phase flow losses, it may be desirable to use an inclusion material that will both react exothermically with aluminum and also forms fewer condensed phase products. The inclusion of fluorocarbons could potentially meet both of these requirements.

Fluorocarbon inclusions, such as polytetrafluoroethylene (PTFE), are of particular interest for three reasons. First, the gravimetric (9.7 kJ/g) and volumetric (20.5 kJ/cm^3) reaction enthalpy of Al/PTFE is high [28]. Second, fluorination of aluminum results in decreased condensed phase products (and potentially lower two-phase flow losses) since AlF_3 sublimates at 1277 °C (1 atm) compared to Al_2O_3 which boils at ~3000 °C. Third, sublimation of AlF_3 formed from reactions within composite particles may break-up particles resulting in reduced agglomeration. Recently, we have shown that low level inclusion of either PTFE [21] or poly(carbon monofluoride) [22] in aluminum via a top-down, readily scalable mechanical activation technique [29] results in tailored, fuel-rich, nanofeatured, micron scale particles with lower specific surface areas than nanoaluminum based compositions, higher combustion enthalpies (20.2–28.7 kJ/g), and enhanced reactivity. Particles with PTFE inclusion are also insensitive, having ESD, impact, and friction ignition thresholds of 90 mJ, >213 cm, and >360 N, respectively [21] and therefore should not adversely affect the sensitivity of formulated propellants.

The objective of this work is to explore how tailored aluminum particles can modify agglomeration in a composite solid propellant. This is achieved by quantifying the effects of aluminum replacement with inclusion modified, fuel-rich Al/PTFE (90/10 and 70/30 wt.%) composite particles. To this end, the effects of inclusion content, particle geometry, and size on propellant characteristics (density and viscosity), theoretical propellant performance, burning rate, metal particle ignition, agglomeration, and metal combustion efficiency are all addressed to determine how PTFE inclusion alters propellant agglomeration.

2. Methods

Thermochemical equilibrium calculations were performed on Al/PTFE mixtures and AP/HTPB propellant formulations containing Al/PTFE using the Cheetah 6.0 equilibrium code so [28] that the effect of PTFE inclusion on condensed phase products and flame temperature could be determined. For propellant calculations, aluminum was replaced with PTFE in a propellant containing 71 wt.% ammonium perchlorate (AP), 14 wt.% hydroxyl-terminated polybutadiene (HTPB), and 15 wt.% of either aluminum or fuel-rich Al/PTFE composite. A chamber pressure of 6.9 MPa and ideal expansion to equilibrium products at 0.1 MPa was assumed.

Ten-gram batches of Al/PTFE composite particles were produced from fuel-rich mixtures of either 90 or 70 wt.% aluminum (35 μm, Valimet H30) and 10 or 30 wt.% PTFE (35 μm, Sigma-Aldrich 468096) via mechanical activation. For safety, mechanical activation was done remotely using 60 mL polypropylene containers (McMaster-Carr 42905T23) using a charge ratio of 12 (73 wt.% 0.95 cm (McMaster-Carr 9529K19), 27 wt.% 0.476 cm (McMaster-Carr 9529K13) 440C steel media) following procedures similar to those previously developed [21]. Specifically, containers were filled with argon (99.997%) prior to mechanical activation on a SPEX 8000 M high energy mill using a duty cycle of 1 min ON, 4 min OFF (50 min of total ON time). During milling, the container was cooled using a fan. All milled materials were handled in an argon-filled glove box and were passivated prior to use. This was done by adding enough hexane to fully cover the particles and then slowly evaporating the hexane in air. Prior to incorporation in propellants, the Al/PTFE composite powders were dry sieved between 25 and 75 μm and their size, morphology, and thermal behavior were determined. The size distributions of the sieved MA composite powder as well as similarly sieved reference powders of spherical (Valimet H30) or flake (Poudres Hermillon YX-49) aluminum were verified using a Malvern Mastersizer 2000 with Hydro 2000 μP dispersion unit and isopropyl alcohol as the medium. These size measurements were compared to calculated, equivalent spherical particle diameters. In doing this, particle volumes were calculated from average particle thicknesses and projected surface areas measured using optical microscopy. Calculated particle volume was then used to determine equivalent spherical particle diameters from a sample of 100 measured particles. Sieved powder specific surface area was measured using a Micromeritics Tristar

3000 surface area analyzer and the BET method. The samples (~80 mg) were degassed at 50 °C in ultra high purity nitrogen for 18 h prior to analysis. The thermal behavior of 1.5–3 mg samples of sieved powders as well as nanoaluminum (Novacentrix 80 nm) was determined with a TA Instruments Q600 DSC-TGA over a temperature range of 100–800 °C. A 20 °C/min heating rate and 100 mL/min flow of a 20/80 vol.% O_2/Ar gas mixture were used. A full characterization (particle size, morphology, specific surface area, combustion enthalpy, and reactivity) of unsieved Al/PTFE MA composite powders is reported elsewhere [21].

Propellant consisted of 14 wt.% of a hydroxyl-terminated polybutadiene (HTPB) binder (cured with isophorone diisocyanate), 71 wt.% AP (80 wt.% coarse 200 μm and 20 wt.% fine 20 μm, ATK), and 15 wt.% of either a sieved composite powder (90/10 or 70/30 wt.%) or a reference aluminum powder (spherical, flake, or nanoscale). The propellant was mixed in ~200 g batches for 20 min in a 250 mL container (McMaster-Carr 42905T25) using a LabRam (Resodyn) mixer at 90% intensity. Propellant was deaerated for 15 min at <35 mbar prior to measuring uncured viscosity and temperature using a Brookfield DVII-HD viscometer with T-spindle. The propellant was then packed into 5.8 mm diameter, ~6 cm long cylindrical strand molds and was cured in air at 60 °C for approximately seven days. After curing, the density of the propellant was measured using Archimedes principle, where density is calculated from the mass of an approximately 1-g piece of propellant measured both unsubmerged and submerged in a bath of isopropyl alcohol.

The ignition of aluminum particles at the propellant burning surface was observed at 1 atm pressure using a high speed video camera (Vision Research, Phantom v7.3) with a long distance microscopic optic (Infinity Photo-Optical, K2 lens) at 11,000–20,000 frames/s using a focused, 1000 W Xenon arc lamp source (Newport Corp. #66921) for illumination. Propellant agglomerate products were collected using the inert gas combustion vessel and the device shown in Fig. 1. Briefly, a 23 mm tall propellant strand is ignited using an electrically heated, 24-gauge nickel-chromium wire. Once the propellant strand burns to a prescribed height, a 10 mW helium-neon laser beam shines across the surface of the burning propellant and into a photodiode detector on the other side of the combustion vessel. This simultaneously triggers the video recording (Vision Research, Phantom Miro eX4, 100 frames/s) of the combustion event, as well as the reversal of the voltage polarity to the DC motor. The motor then sweeps a pendulum with an attached borosilicate quench disc (McMaster-Carr 8477K11) past the surface of the burning propellant at a velocity of ~7 m/s and a height of 2–6 mm above the burning surface. During this process agglomerate products from propellant combustion are quenched on the surface of the borosilicate disc, which then moves to the other side of the combustion vessel where it is protected from the combustion product flow for the remainder of the experiment. This unique quenching technique varies from other approaches in literature [7,30,31], and eliminates contamination of the products with the igniter wire, sampling error due to product washing/filtration, and uncertainties in quench height. However, like the quench bath technique [30] and some configurations of the filter capture technique [18], this method may have difficulty capturing fine fraction condensed products. This is a result of fine particles following flow around rather than impacting the disc. Like the quench bath technique, this method does collect fine fraction (<1 μm) products, which as shown in Fig. 10, can be as small as 150 nm. It is unclear whether fine fraction particles impact the plate or are quenched from the gas phase. Regardless, fine condensed products are not the focus of this work, as they do not result in significant two phase flow loss [32]. The borosilicate quench disc is extracted from the experiment and agglomerates are analyzed directly on the same borosilicate surface upon which they were quenched. Surface images were taken using a FEI Quanta 3D-FEG scanning electron microscope (SEM). Agglomerate product size was determined by direct measurement (sample size of 100 agglomerates) similar to Ref. [7]. Agglomerate product phase and composition were also determined using electron dispersive spectroscopy (EDS, Oxford INCA Xstream-2 silicon drift detector) and X-ray diffraction (XRD, Bruker D8 powder difractometer, 2 deg/min scan rate).

3. Results and discussion

Theories suggest that agglomeration in solid propellants is due in part to the large temperature disparity between the aluminum melting (660 °C) and ignition (~2050 °C) temperatures [33]. The large temperature difference results in liquid aluminum droplets having long surface residence times, enabling coalescence prior to ignition and liftoff. This suggests that altering the thermal behavior of aluminum prior to ignition is important to both understanding and reducing agglomeration in a solid propellant. To understand this thermal behavior, differential scanning calorimetry (Fig. 2) of sieved Al/PTFE composite particles and reference

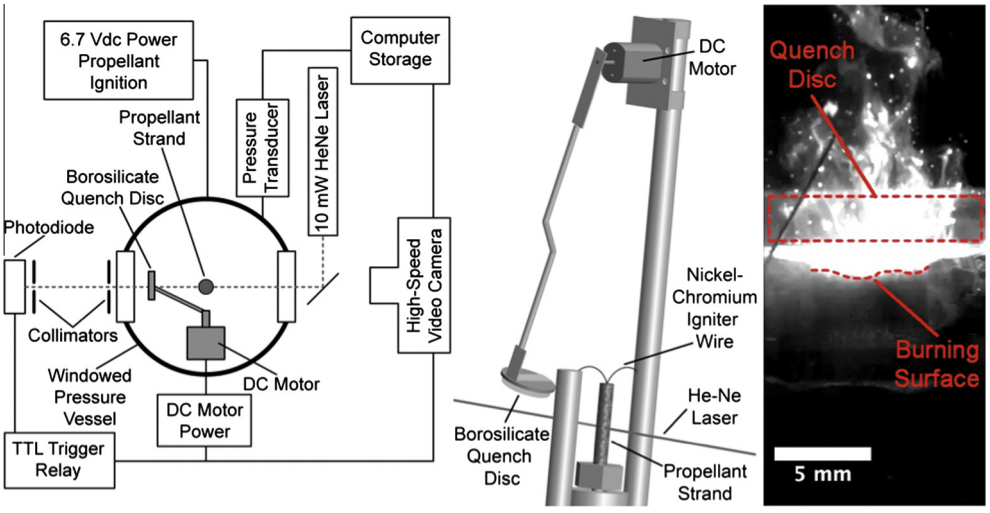

Fig. 1. Diagram of propellant combustion experiment (left), detail showing agglomerate quench device (center), and still frame showing actuation and agglomerate capture (right).

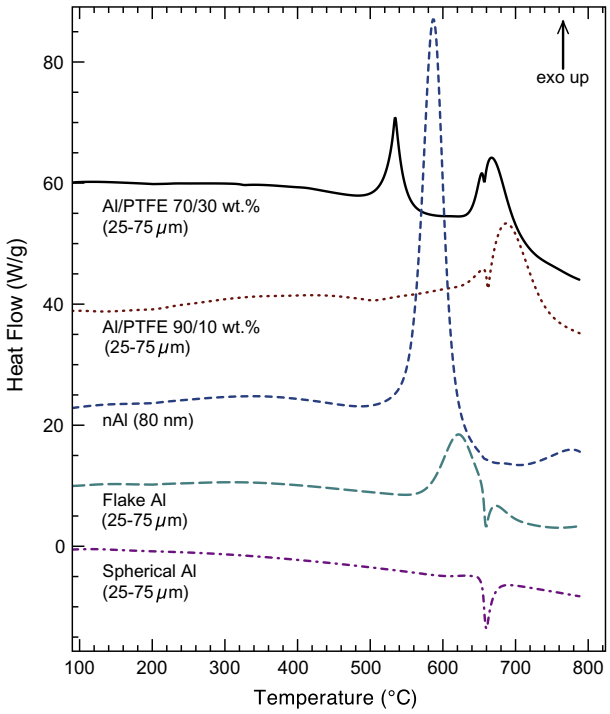

Fig. 2. Differential scanning calorimetry from heating (20 °C/min, 20/80 vol.% O_2/Ar) of sieved Al/PTFE composite particles and reference aluminum particles. Heat flow traces are offset for presentation.

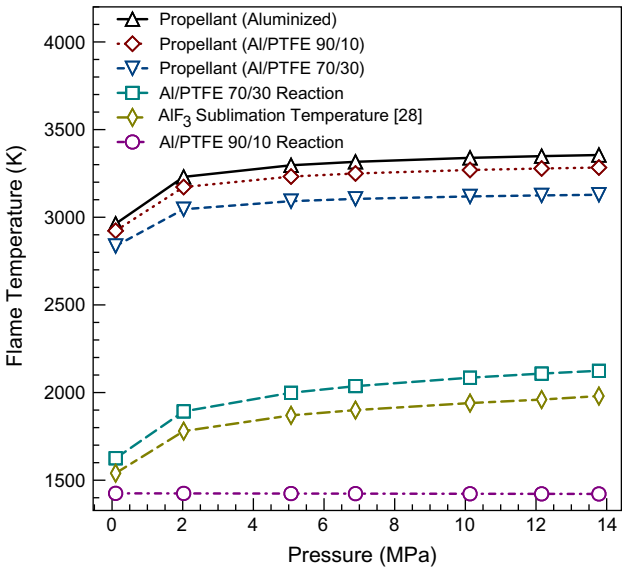

Fig. 3. Computed flame temperatures of Al/PTFE reactions and Al/PTFE containing propellant combustion as a function of gas pressure.

aluminum particles was conducted in O_2/Ar to show the differences in heating characteristics. In heating of spherical aluminum to 800 °C, no perceivable oxidation heat release or weight gain occurs either before or after aluminum melting (660 °C). However, with flake aluminum, oxidation onsets at ~550 °C and results in a 13% weight gain (not shown). This is similar to the experimental and computational findings of Trunov et al. [34]. Similarly, nAl also oxidizes at a temperature lower than the bulk melting temperature (oxidation onsets ~530 °C) and results in more complete oxidation (a 40% weight gain) for the conditions considered. The reaction characteristics of unsieved, mechanically activated Al/PTFE composite particles (70/30 wt.%) are discussed in detail in previous work [21]. For sieved Al/PTFE 90/10 wt.% composite particles, a broad exotherm accompanied by weight gain (~8%, not shown) onsets around 500 °C as a result of simultaneous reaction of oxygen and PTFE decomposition products with aluminum. Oxidation is further accelerated by the aluminum melting and results in an overall weight gain of 16%. Additional PTFE inclusion (Al/PTFE 70/30 wt.%) within composite particles results in a strong exotherm (onsetting ~500 °C) that is initiated by PTFE decomposition and reaction (a 16% weight loss), while a second exotherm (onsetting ~630 °C) results in a 15% weight gain due to aluminum oxidation. Additionally, as noted elsewhere [21], at temperatures below the melting point of PTFE (327 °C), heating of Al/PTFE (90/10 and 70/30 wt.%) particles may cause intra-particle strain due to differences in the aluminum and PTFE thermal expansion coefficients. In a propellant, this could lead to delamination of the aluminum and PTFE layers, which could contribute to particle breakup during ignition.

The ignition behavior of Al/PTFE composite particles are strongly affected by PTFE inclusion level and insight into these differences can be drawn from equilibrium calculations of both Al/PTFE reactions and of propellants containing Al/PTFE. Exclusive reaction of aluminum with PTFE is of interest as it likely occurs prior to significant aluminum reaction with the surrounding oxidizer. Therefore, we perform thermochemical equilibrium calculations of aluminum and PTFE only to gain insight into these first reactions. Further, the PTFE inclusion level determines whether or not heat generated from the Al/PTFE reaction alone is sufficient to produce gaseous products. In examining the Al/PTFE adiabatic flame temperature as a function of both PTFE inclusion level and gas pressure (Fig. 3), it is evident that use of 30 wt.% rather than 10 wt.% PTFE leads to drastically higher flame temperatures. In fact, the reaction of Al/PTFE 90/10 wt.% mixtures results in exclusively condensed phase products and a temperature of 1425 K that is insensitive to pressure. In contrast, for 70/30 wt.% mixtures at typical rocket motor pressures (up to ~13 MPa), the predicted reaction temperature is above the computed AlF_3 sublimation temperature and theoretically results in gaseous AlF_3 formation, which suggests that unlike 90/10 wt.% Al/PTFE particles, heat generated from reaction within 70/30 wt.% particles could produce gaseous AlF_3 inside particles, resulting in internal pressurization and particle breakup. The differences in these two ignition mechanisms are consistent with observations from butane torch ignition of these two types of inclusion-modified particles in air (see Supplemental video #1), where combustion of 90/10 wt.% particles results in a slow, condensed phase reaction and combustion of 70/30 wt.% particles results in significant gas production, dispersion, and rapid combustion.

As well as affecting aluminum ignition, addition of PTFE to a solid propellant may have a significant effect on overall propellant combustion. As shown in Fig. 3, the computed adiabatic flame temperature of aluminized propellant (15 wt.% Al, 14 wt.% HTPB, 71 wt.% AP) is 3300 K at 6.9 MPa, but is reduced to 3250 K or 3100 K by replacement of aluminum with either 90/10 wt.% or 70/30 wt.% Al/PTFE, respectively. This lower adiabatic flame temperature decreases the theoretical specific impulse (Fig. 4) from 262.5 s (no PTFE) to either 260.6 s (10 wt.% PTFE) or 255.5 s (30 wt.% PTFE). These theoretical specific impulse calculations do not take into account potential performance improvement that could result from smaller agglomerate size (reduced two-phase flow loss). As such, it is possible performance improvements from reduced two-phase flow loss may exceed this two to seven second (0.8–2.7%) decrease in theoretical specific impulse. For propellant applications the amount of PTFE should be minimized for optimized theoretical performance. The amount of PTFE could be

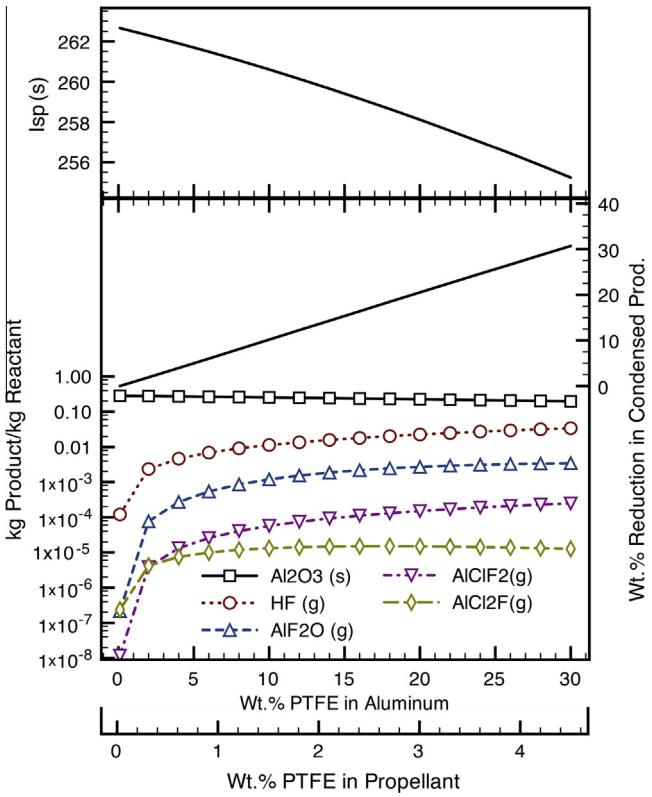

Fig. 4. Ideal specific impulse, selected exhaust products, and reduction in condensed phase product formation for propellant combustion (6.89 MPa chamber, ideal expansion to 0.1 MPa) as a function of PTFE inclusion level.

reduced some from 30% and still result in gas production that would aid in particle breakup. but these calculations suggest that 10 wt.% PTFE does not result in gaseous AlF_3 formation exclusively from Al/PTFE reaction.

Regardless of whether or not Al/PTFE reaction produces gaseous AlF_3, the high flame temperatures in a rocket environment will result in sublimation of any condensed phase AlF_3, and will significantly decrease condensed phase exhaust products. Examination of the dominant computed propellant exhaust products (Fig. 4) indicates 30 wt.% PTFE inclusion (4.5% of propellant weight) decreases the solid alumina product mass from 0.28 to 0.19 kg/kg propellant. Addition of PTFE also results in a number of gaseous species being formed such as HF and several other gaseous aluminum fluorides, aluminum fluoride oxides, and aluminum chloride fluorides. The most prevalent of these aluminum fluoride oxides and aluminum chloride fluorides are AlF_2O, $AlClF_2$, and $AlCl_2F$ (Fig. 4), which upon further cooling and expansion to 0.01 MPa (not shown), combine with dissociated species and convert to gaseous AlF_3 and HF. Overall, predictions indicate use of 70/30 wt.% Al/PTFE instead of aluminum in propellant decreases the condensed phase exhaust product mass by 30%.

In addition to thermochemical behavior, it is expected that morphology, size distribution, and surface area of composite particles is important. The composite and reference aluminum powders exhibit several distinct size and morphological differences. Single particle scanning electron microscope (SEM) images (Fig. 5) show that the morphology of Al/PTFE composite particles and flake aluminum are very different from either nAl or spherical aluminum. While flake aluminum particles appear to have a relatively smooth surface, the surfaces of Al/PTFE composite particles (both 90/10 and 70/30 wt.%) are more highly featured due to cold welding of alternating layers of aluminum and PTFE. Though not shown in SEM images, Al/PTFE composite particles are generally thicker (~12 μm) than flake aluminum particles (~6 μm). These variations in particle morphology lead to differences in sieving efficiency of the particles. All powders except the 80 nm nAl were sieved to 25–75 μm and laser scattering measured size distributions (Fig. 5) show that a small portion of the Al/PTFE composite particle and flake aluminum distributions are below ~20 μm in size and that these distributions are broader than that of spherical aluminum. As well as differences in sieving efficiency, the assumption that particles are spherical, which is necessary to obtain a particle size distribution using Fraunhofer scattering theory also contributes to differences in size distributions. However, the average particle sizes of both 90/10 and 70/30 wt.% composite particles (31.3, 42.3 μm) as well as the average size of flake aluminum (30.6 μm) are all comparable to spherical aluminum (43.3 μm), and are far larger than the average size of nAl. The average particle size measured from laser scattering is also close to the equivalent spherical diameter of particles measured from the projected area of particles observed in an optical microscope. For flake and Al/PTFE (90/10 and 70/30 wt.%) particles, these equivalent diameters are 34.2, 38.1, and 40.7 μm, respectively. The differences in geometry and morphology also affect the particle specific surface area (Table 1). The specific surface area of spherical aluminum particles is low (0.051 m^2/g), while both flake and nAl have higher surface areas (3.58 and 25.7 m^2/g, respectively). The specific surface areas of both 90/10 and 70/30 wt.% Al/PTFE composite particles (2.55 and 2.48 m^2/g, respectively) are far lower than that of nAl and are lower than that of flake aluminum.

These variations in particle size distribution, morphology, and specific surface area have a significant effect on propellant properties (Table 1). The non-spherical morphology and higher specific surface areas of the Al/PTFE composite particles and flake aluminum result in a near factor of ten increase in mix viscosity from 4.8×10^6 cP (spherical Al) to 4.8×10^7 cP (flake Al), 3.7×10^7 cP (Al/PTFE 90/10 wt.%), or 4.2×10^7 cP (Al/PTFE 70/30 wt.%). However, the viscosities of Al/PTFE and flake aluminum-containing propellants are nearly half the viscosity of propellant containing 80 nm nAl (8.8×10^7 cP). Regardless of their higher viscosity, processability of propellants containing Al/PTFE composite particles was acceptable. The cured densities of propellants containing both 90/10 wt.% Al/PTFE (1.70 g/cm^3, 88.7% TMD) and 70/30 wt.% Al/PTFE (1.72 g/cm^3, 90.6% TMD) were comparable to the density of the propellant containing spherical aluminum (1.68 g/cm^3, 87.6% TMD). However, the densities of propellant containing flake aluminum (1.66 g/cm^3, 85.6% TMD) and nAl (1.64 g/cm^3, 83.6% TMD) were lower, suggesting an inability of the binder to wet the entire surface area of these particles during propellant mixing. Although not quantified here, the sensitivity of propellants containing modified aluminum particles are expected to be acceptable, as the composite particles themselves are insensitive to impact, friction, and electrostatic discharge ignition [21] and the addition of a binder in a formulated propellant is not expected to increase sensitivity.

Images of propellants burning at 1 atm pressure (Fig. 6) show PTFE inclusion results in drastic differences in particle ignition and burning particle size. Considering first propellant containing spherical aluminum particles, very little aluminum combustion is observed at the surface and most aluminum combustion begins only after particles have traveled ~2 mm from the propellant surface. This results in a dark region near the burning surface of the propellant as shown (Fig. 6). Conversely, flake aluminum particles remain attached to the burning surface during ignition and have longer surface residence times, which promotes coalescence into agglomerates. These agglomerates leave the surface and burn with a bright, visible flame and aluminum oxide smoke product trail. Nanoscale aluminum on the other hand promptly ignites at the surface and forms visible agglomerates. The faster burning rate of

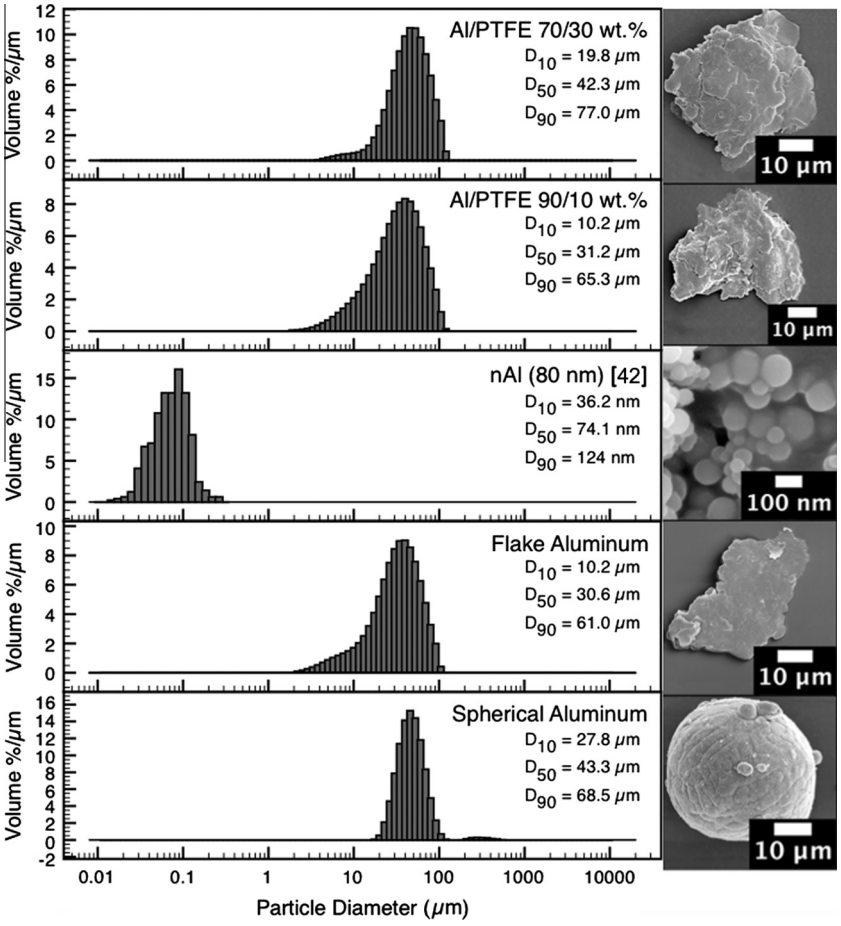

Fig. 5. Volume weighted particle size distributions of 25-75 μm sieved MA particles and spherical, flake, and nanoscale [42] reference aluminum powders (left) measured using laser diffraction. Electron micrographs (right) show the morphology of particles.

Table 1
Al/PTFE or aluminum particle specific surface area, propellant formulation details, uncured viscosity, and cured density. All propellants contain 71 wt.% AP (80 wt.% 200 μm coarse, 20 wt.% 20 μm fine), 14.0 wt.% HTPB binder, and 15 wt.% aluminum or MA composite (25–75 μm).

Propellant designation	Metal type	Metal SSA (m^2/g)	Propellant metal content (wt.%)	Uncured viscosity (30–35 °C) (cP)	Cured density (g/cm^3)	Cured density (%TMD)
Spherical	Spherical Al	0.051[a]	15	4.8×10^6	1.68	87.6
Flake	Flake Al (YX-49)	3.58	15	4.8×10^7	1.66	85.8
nAl	Nanoaluminum, 80 nm	25.7[b]	15	8.8×10^7	1.64	83.6
90/10	Al/PTFE 90/10 wt.%, 50 min MA	2.55	15	3.7×10^7	1.70	88.7
70/30	Al/PTFE 70/30 wt.%, 50 min MA	2.48	15	4.2×10^7	1.72	90.6

[a] Calculated specific surface area.
[b] Manufacturer reported specific surface area.

nAl containing propellant at 1 atm pressure (2.6 cm/s) in comparison to propellants containing spherical, flake aluminum, or composite particles (1.5 cm/s) contributes to the considerably brighter combustion and greater number density of burning agglomerates apparent in nanoaluminized propellant combustion. Similar to propellants containing nAl and flake aluminum, use of Al/PTFE composite particles (both 90/10 and 70/30 wt.%) results in prompt particle ignition at the burning surface and small burning particles. This is more pronounced when composite particles with 30 wt.% PTFE inclusion are used. Video of the combustion process (see Supplemental video #2) shows that mechanically activated particles leave the propellant surface at velocities as high as ~13 m/s, which is faster than agglomerates from spherical aluminized propellant (~3.8 m/s). Since burning rates of propellants containing spherical aluminum, flake aluminum, or Al/PTFE particles are all similar, the higher velocity of burning Al/PTFE composite particles cannot be explained by a higher burning rate alone and implies that these agglomerates are smaller than those produced from spherical aluminized propellant such that velocities of the particles and gas are more similar.

Closer examination of the burning surface of propellant containing Al/PTFE composite particles reveals that the mechanism responsible for smaller burning particles appears to be the breakup of composite particles during ignition and subsequent combustion. During Al/PTFE particle heating, disparate thermal expansion of the aluminum and PTFE may help separate Al/PTFE particles into fragments. Subsequent Al/PTFE particle reaction can then produce AlF_3 gas at Al/PTFE interfaces throughout the interior of the

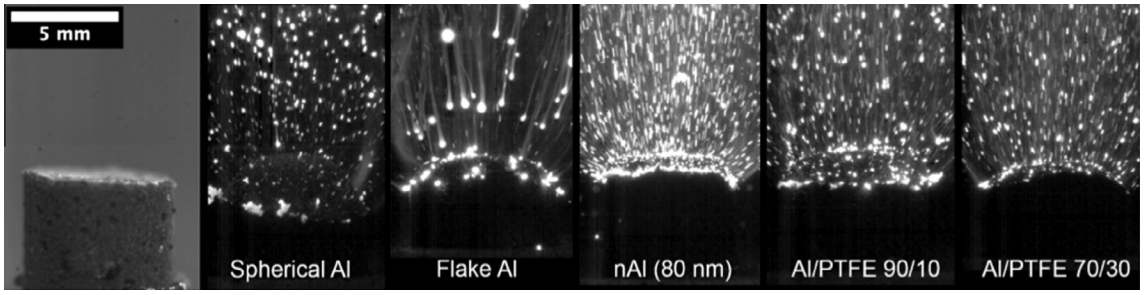

Fig. 6. Solid propellant pellet (left) and burning surfaces of pellets containing sieved spherical, flake, 80 nm nAl, Al/PTFE 90/10 wt.%, and Al/PTFE 70/30 wt.% (right). Pressure is 0.1 MPa and all photos were taken with the same exposure settings.

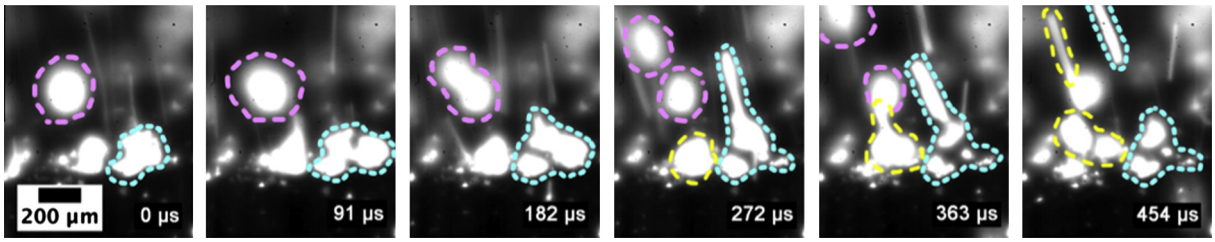

Fig. 7. Image sequence of the burning surface of an Al/PTFE 70/30 wt.% containing propellant (0.1 MPa) showing breakup of three large agglomerates at the surface (pink, blue and yellow dashed outlines). Much smaller particles (~20 µm or smaller) can be seen throughout the image sequence, igniting and leaving the surface at high velocity. (For interpretation of the references to color in this figure legend, the reader is referred to the web version of this article.)

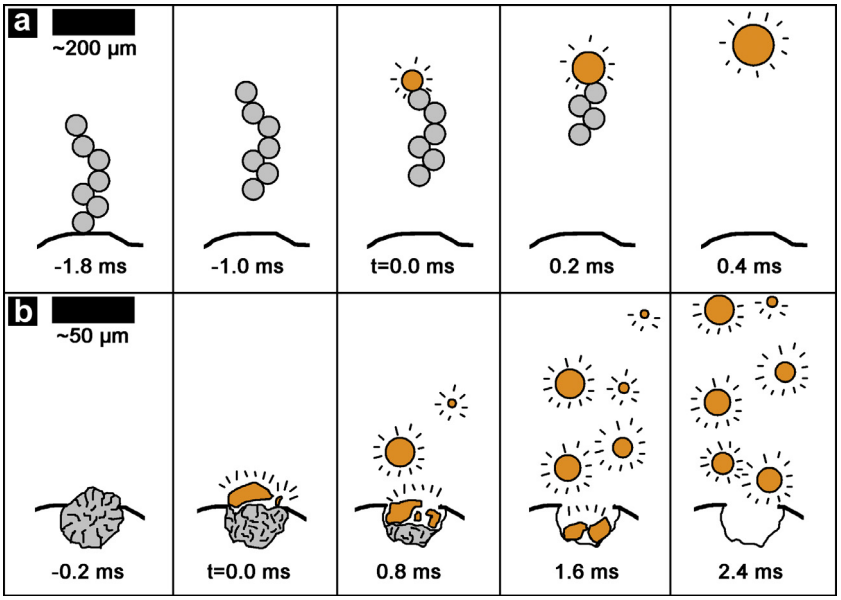

Fig. 8. Schematic of the burning surface metal particle ignition mechanism for propellants containing (a) spherical aluminum and (b) Al/PTFE 70/30 wt.% composite particles. Times and sizes are approximate.

particles, resulting in breakup into smaller particles having shorter burning times. This breakup process is observed in a high magnification image sequence (Fig. 7) and in Supplemental video #2, where the burning surface of Al/PTFE 70/30 wt.% propellant is shown. Here, numerous small fragments of Al/PTFE particles (<20 µm) can be seen igniting and separating from the propellant surface. In addition to these small fragments, three larger (~200 µm diameter) agglomerates can be seen in the image sequence breaking up into multiple smaller, 50–100 µm diameter fragments likely as a result of AlF_3 sublimation caused by heating. This is in contrast to the propellant containing similarly sized flake aluminum, where large agglomerates and no breakup are observed. The breakup process is schematically shown in Fig. 8 where it is contrasted to the ignition and agglomeration of spherical aluminum (also shown in Supplemental video #2).

Scanning electron micrographs (Fig. 9) of quenched combustion products from reference aluminized propellants clearly show the differences in agglomeration that result from aluminum particle morphology and size. Products contain both a visible, coarse fraction and a fine fraction (<1 µm, not visible in Fig. 9). As only the coarse fraction typically results in significant two-phase flow losses [32], analysis and agglomerate size measurement focuses

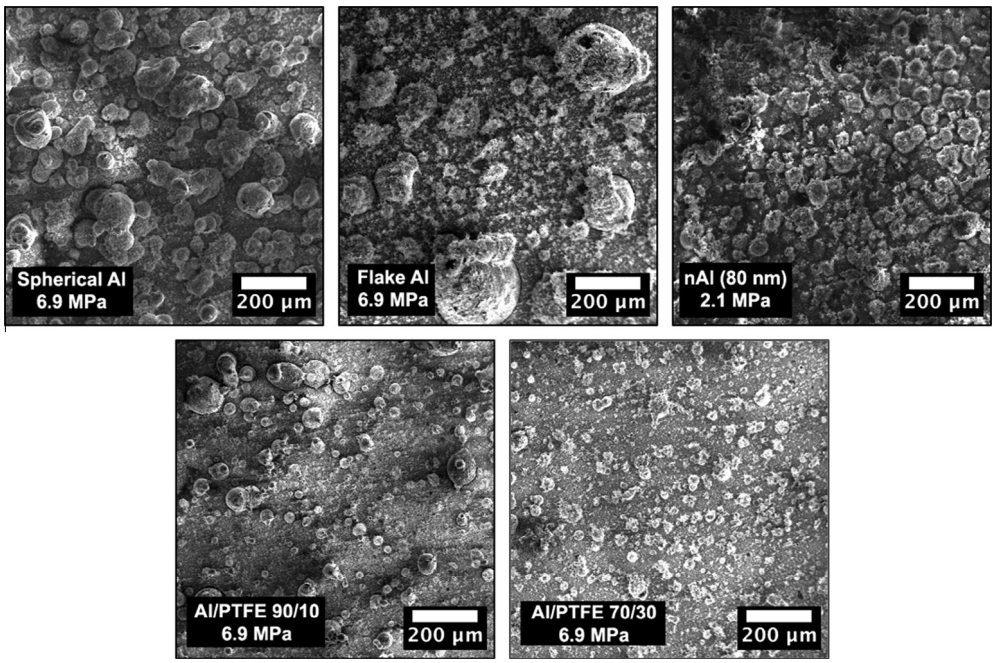

Fig. 9. Electron micrographs of quenched coarse fraction agglomerates from 6.9 or 2.1 MPa combustion of propellant containing 25–75 µm particles of spherical aluminum, flake aluminum, nAl, or Al/PTFE composite particles.

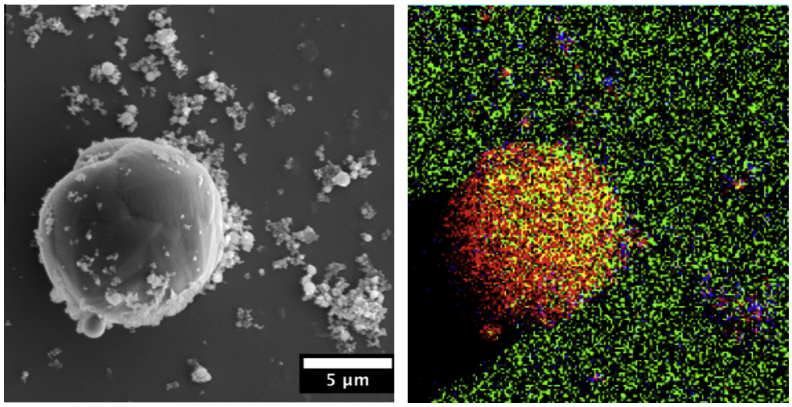

Fig. 10. Electron micrograph (left) and EDS chemical map (right) of coarse and fine fraction quenched products from Al/PTFE 70/30 wt.% composite particle containing propellant burned at 6.9 MPa. In EDS map, aluminum = red, oxygen = green, fluorine = blue. (For interpretation of the references to color in this figure legend, the reader is referred to the web version of this article.)

on the coarse fraction only. Products from combustion of spherical aluminized propellants contain many coarse, spherical agglomerates that are slightly larger than the initial aluminum size (25–75 µm) and are covered by a layer of the fine fraction particles. In general, the amount of condensed product present from combustion of spherical aluminized propellant is high. Coarse agglomerates collected from flake aluminized propellant are even larger in size with some agglomerates on the order of ~200 µm. This is likely a result of long residence time on the propellant surface, which contributes to agglomeration. Use of nanoaluminum does result in smaller agglomerates than flake or spherical aluminized propellants, but agglomeration is still significant, as the volume fraction of the coarse agglomerates is high and agglomerates are orders of magnitude larger than the size of nanoaluminum. A high degree of agglomeration has been seen in combustion of other nanoaluminized propellants [7–9], and is predicted by molecular dynamic simulations of metal nanoparticle sintering and coalescence [10]. It should be noted that nanoaluminized propellant agglomerates were collected at a gas pressure of 2.1 MPa instead of 6.9 MPa because these propellants burned unreliably and too quickly to enable agglomerate capture at 6.9 MPa and higher pressures. This was largely due to lower propellant density and poor mechanical strength. As agglomerate size is inversely related to gas pressure [35,36], agglomerate sizes from nanoaluminized propellant are not directly comparable to those of other propellants collected at 6.9 MPa. As such, these data may overestimate the degree of agglomeration occurring from nanoaluminized propellant combustion. However, average agglomerate sizes previously reported for nanoaluminized composite propellant indicate agglomerates are also orders of magnitude larger than the original nAl particle sizes, with reported average agglomerate sizes varying from 1–3 µm [7] to 20 µm [8].

Aluminum/PTFE composite particles result in noticeable reductions in both coarse agglomerate diameter and coarse product fraction. The small size of products from Al/PTFE (90/10 wt.%) aluminized propellants (Fig. 9) show that condensed AlF_3

formation within Al/PTFE particles and subsequent sublimation can also break apart agglomerates. Additional inclusion material (70/30 wt.%) further reduces coarse product size, indicating that AlF_3 gas formation directly from Al/PTFE reaction reduces product particle size even further. Much less coarse product is observed for both of these cases, which is due to higher number of small product particles as well as the reduced condensed phase product mass fraction (30 wt.% lower theoretically). Higher magnification examination of quenched products from propellants containing Al/PTFE 70/30 wt.% composite particles (Fig. 10) shows both the coarse and the fine, sub-micrometer product fractions. Electron dispersive spectroscopy of these products indicates the coarse fraction is made up of aluminum and oxygen, while the fine fraction consists of aluminum, oxygen, and fluorine. The atomic ratios of aluminum to oxygen (not shown) suggest that the coarse fraction is completely oxidized. The absence of crystalline aluminum in Al/PTFE 70/30 wt.% propellant products is also confirmed by XRD (Fig. 11). This indicates aluminum combustion is completed very near the burning surface, and is consistent with the observed smaller burning particles. Additionally, the presence of aluminum fluoride is confirmed in combustion products from propellant containing Al/PTFE 70/30 wt.%. Conversely, use of spherical aluminum forms products that contain a significant amount of unreacted, crystalline aluminum as well as traces of unreacted ammonium perchlorate. For both propellants the products also contained a number of different aluminum oxide phases.

Direct measurement of the coarse fraction particles (Fig. 12) shows the degree to which coarse product size is affected by initial aluminum particle size, geometry, and PTFE inclusion level. The coarse agglomerate fraction from propellant containing spherical aluminum (burned at 6.9 MPa) is lognormally distributed with a 76 μm average diameter. Agglomerates from flake aluminized propellant are much larger (125 μm average diameter) and have a broader distribution. As discussed previously, the larger agglomerate size is an effect of long surface residence time caused by flake geometry. Nanoaluminized propellant (burned at 2.1 MPa) produces smaller agglomerates (55.2 μm average diameter), though these agglomerates are several orders of magnitude larger than the initial nAl diameter. Agglomerates from propellant containing Al/PTFE 90/10 wt.% composite particles (burned at 6.9 MPa) have an average particle size of 54.7 μm. Further inclusion of PTFE (70/30 wt.% composite particles) in propellant burned at 6.9 MPa results in smaller product particles (25.4 μm average diameter), that are smaller than the initial average size of Al/PTFE 70/30 wt.% particles (42.3 μm). In comparison to both spherical and flake aluminized propellant agglomerates, this is a reduction in average agglomerate diameter of 66% and 80%, respectively (corresponding agglomerate volume decreases of 96% and 99%, respectively). This shows that regardless of the flake-like geometry of Al/PTFE particles, breakup of particles at the surface through AlF_3 gas production (either from ignition or from subsequent heating) can result in much smaller condensed phase products. In general, these results show that fluorocarbon inclusion can result in product agglomerates that are smaller than the starting particle size and a reduction in coarse agglomerate fraction as discussed above.

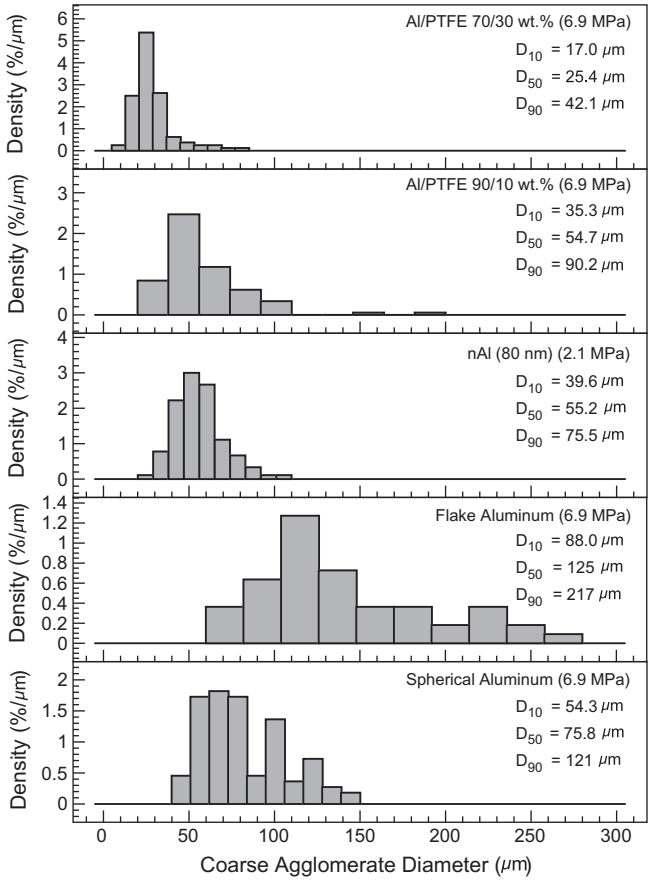

Fig. 12. Size distributions of coarse fraction agglomerate products from propellant combustion (6.9 or 2.1 MPa). Sample size, $n = 100$ for each distribution.

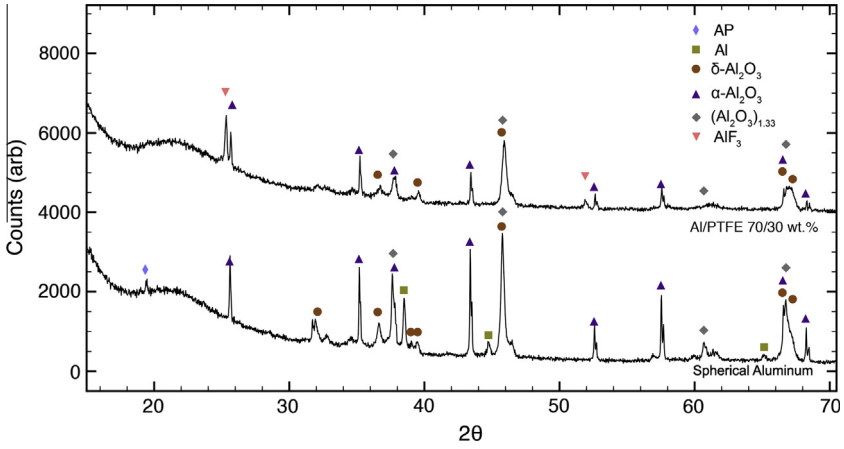

Fig. 11. X-ray diffraction phase composition of products quenched during combustion (6.9 MPa) of propellant containing spherical aluminum particles (bottom) and Al/PTFE 70/30 wt.% composite particles (top).

As might be expected, the aluminum particle morphology and size correlates to the propellant burning rates for spherical, flake, and nanoscale aluminized propellants (Fig. 13). Spherical and flake aluminized propellant burning rate pressure dependencies (0.36 and 0.37, respectively) are nearly identical; however, their pre-exponents (0.49 and 0.56) differ appreciably. The small thickness of the flake aluminum used in this study (~6 μm thick, ~30 μm diameter) appears to have a similar effect on propellant burning rate as nAl [37]. Specifically, both lead to an increase in propellant burning rate pre-exponent only. This idea is further supported by DSC/TGA oxidation of flake aluminum (discussed previously), where similar to nAl, appreciable flake aluminum oxidation occurs below the melting temperature of bulk aluminum. It is worth noting that in work reported by Meda et al. [37], replacement of 30 μm spherical aluminum with larger, 50 μm, flake aluminum did not result in a pre-exponent shift, but flake thickness was not reported and could be larger than the flake aluminum used in this work. Likewise, nanoaluminized propellant burning rates obtained by others [9,37] suggest replacement of spherical aluminum with nAl also results in an increase in pre-exponent only. However, in this work, the burning rate of nanoaluminized propellant (1.22 cm/s) was obtained at 2.1 MPa only, and burning rates could not be determined at higher pressures due to sporadic, unreliable propellant combustion resulting from poor propellant density.

Though aluminum size and morphology change propellant burning rate pre-exponent, the effects of PTFE inclusion are more pronounced. For low inclusion levels (replacement of spherical aluminum with Al/PTFE 90/10 wt.%), composite particles have no effect on either burning rate pre-exponent or pressure sensitivity. This is expected, as Al/PTFE 90/10 wt.% composite particles (~12 μm thick) are twice the thickness of flake aluminum and unlike 70/30 wt.% composite particles, do not immediately separate into smaller particles as a result of Al/PTFE reaction. However, further PTFE inclusion (30 wt.%) does dramatically increase the pressure dependence from 0.36 to 0.58, which at 13.8 MPa results in a 50% increase in burning rate (Fig. 12). This increased pressure dependence is believed to be a result of the greater influence of kinetics that likely occurs from smaller Al/PTFE 70/30 wt.% coarse agglomerate products (25.4 μm average diameter) burning relatively close to the surface. These products suggest the presence of small (~10–20 μm) burning aluminum particles. In separate work, aluminum particles of this size have been experimentally observed to transition from diffusion to kinetic controlled combustion [3–6,38–41]. Consistent with findings presented here, it has been shown elsewhere [6] using a simple analysis that kinetically controlled particle burning results in higher burning rate pressure dependence compared to diffusionally controlled burning. While a higher pressure exponent is of interest for some applications, it may increase motor instability. For applications where stability is of concern, 90/10 wt.% composite particles may be preferred.

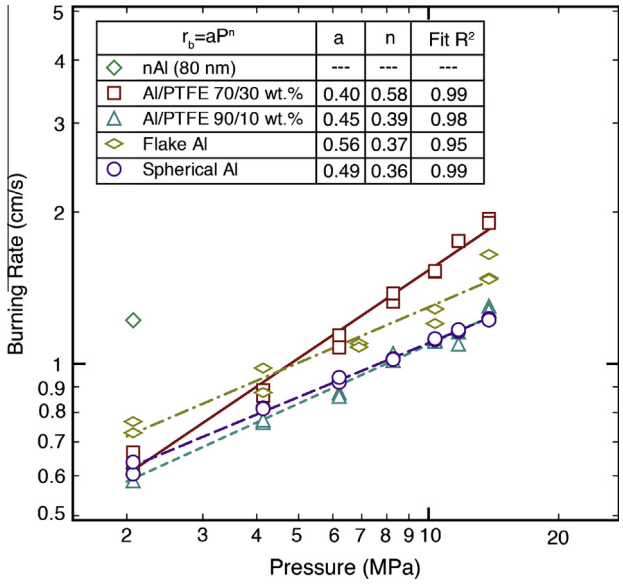

Fig. 13. Solid propellant linear burning rates and power law pressure dependence.

4. Conclusions

In summary, this work shows that the use of tailored Al/PTFE composite particles can result in drastic alteration of solid propellants burning characteristics which may decrease two-phase flow losses in rocket motors. Breakup of the particles is thought to be due to both intraparticle gas production and the disparate thermal expansion properties of the aluminum and PTFE. The overall smaller, faster (mass) burning of particle fragments that ignite promptly at or near the propellant surface results in improved heat transfer back to the propellant. This also results in more complete aluminum combustion near the propellant surface and faster burning rates. Additionally, these smaller particles can result in more kinetically limited aluminum combustion and a greater dependence of burning rate on pressure. Similarly, 10 wt.% PTFE inclusion can alter particle ignition and reduce coarse agglomerate fraction and size. However, unlike 30 wt.% PTFE, 10 wt.% PTFE inclusion does not affect propellant burning rate. Finally, because Al/PTFE (90/10 and 70/30 wt.%) particles breakup during or after ignition, they can produce agglomerates that are smaller than even the initial composite particles. In comparison to similarly sized spherical and flake aluminum, Al/PTFE inclusion modified particles (70/30 wt.%) result in a reduction in average coarse fraction agglomerate size from either 75.8 or 125 μm, respectively to 25.4 μm, which are 96% and 99% decreases in agglomerate volume, respectively. Addition of either 10 or 30 wt.% PTFE inclusion result in 0.8% or 2.7% reductions in predicted specific impulse, but the drastic reduction in coarse agglomerate size may exceed this specific impulse loss by reducing two-phase flow losses in a motor.

Current and future efforts are focused on use of other inclusion materials that result in net increases to theoretical Isp performance. Strategies to reduce propellant viscosity will also be explored and include the use of larger mechanically activated particles as well as control of composite particle geometry. Future work will also study the ignition of these composite particles at high heating rates using a variety of techniques.

Acknowledgments

The authors would like to acknowledge the financial support of the Air Force Office of Scientific Research MURI under the supervision of Dr. Mitat Birkan (#FA9550-13-1-0004).

Appendix A. Supplementary material

Supplementary data associated with this article can be found, in the online version, at http://dx.doi.org/10.1016/j.combustflame.2013.08.009.

References

[1] G.P. Sutton, O. Biblarz, Rocket Propulsion Elements, seventh ed., Wiley, Hoboken, NJ, 2001.
[2] H. Cheung, N.S. Cohen, AIAA J. 3 (1965) 250–257.
[3] R.A. Yetter, G.A. Risha, S.F. Son, Proc. Combust. Inst. 32 (2009) 1819–1838.
[4] M.W. Beckstead, Combust. Explos. Shock Waves 41 (2005) 533–546.
[5] T. Bazyn, H. Krier, N. Glumac, Proc. Combust. Inst. 31 (2007) 2021–2028.
[6] C.R. Zaseck, S.F. Son, T.L. Pourpoint, Combust. Flame 160 (2012) 184–190.

[7] K. Jayaraman, S.R. Chakravarthy, R. Sarathi, Proc. Combust. Inst. 33 (2011) 1941–1947.
[8] V. Babuk, I. Dolotkazin, A. Gamsov, A. Glebov, L.T. DeLuca, L. Galfetti, J. Propul. Power 25 (2009) 482–489.
[9] L. Galfetti, L.T. DeLuca, F. Severini, G. Colombo, L. Meda, G. Marra, Aerosol Sci. Technol. 11 (2007) 26–32.
[10] M.R. Zachariah, M.J. Carrier, J. Aerosol Sci. 30 (1999) 1139–1151.
[11] K. Jayaraman, K.V. Anand, D.S. Bhatt, J. Propul. Power 25 (2009) 471–481.
[12] S. Cerri, M.A. Bohn, K. Menke, Propellants, Explos., Pyrotech. 38 (2013) 190–198.
[13] D.T. Bui, A.I. Atwood, T.M. Antienza-More, Effect of aluminum particle size on combustion behavior of aluminized propellants in PCP binder, in: 35th International Annual Conference of ICT, Karlsruhe, 2004.
[14] O. Orlandi, J.F. Guery, G. Lacroix, S. Chevalier, N. Desgardin, HTPB/AP/Al Solid propellants with nanometric aluminum, in: European Conference for Aerospace Sciences (EUCASS), Moscow, 2005.
[15] Y. Yavor, A. Gany, Effect of nickel coating on aluminum combustion and agglomeration in solid propellants, in: 44th AIAA/ASME/SAE/ASEE Joint Propulsion Conference & Exhibit, Hartford, CT, 2008.
[16] V. Babuk, V. Vassiliev, V. Sviridov, Combust. Sci. Technol. 163 (2001) 261–289.
[17] L.T. DeLuca, E. Marchesi, M. Spreafico, Int. J. Energ. Mater. Chem. Propul. 9 (2010) 91–105.
[18] O.G. Glotov, D.A. Yagodnikov, V.S. Vorob'ev, V.E. Zarko, V.N. Simonenko, Combust. Explos. Shock Waves 43 (2007) 320–333.
[19] J.D.E. White, R.V. Reeves, S.F. Son, A.S. Mukasyan, J. Phys. Chem. A 113 (2009) 13541–13547.
[20] V.A. Babuk, V.A. Vassiliev, V.V. Sviridov, in: V. Yang, T.B. Brill, W.Z. Ren, P. Zarchan (Eds.), Solid Propellant Chemistry, Combustion, and Motor Interior Ballistics AIAA, 2000, p. 749–776.
[21] T.R. Sippel, S.F. Son, L.J. Groven, Propellants, Explos., Pyrotech. 38 (2013) 286–295.
[22] T.R. Sippel, S.F. Son, L.J. Groven, Propellants, Explos., Pyrotech, 2013, doi: http://dx.doi.org/10.1002/prep.201200202.
[23] D. Stamatis, X. Jiang, E. Beloni, E.L. Dreizin, Propellants, Explos., Pyrotech. 35 (2010) 260–267.
[24] D.A. Reese, L.J. Groven, S.F. Son, A.S. Mukasyan, Intermetallic compounds as fuels for composite rocket propellants, in: 47th AIAA/ASME/SAE/ASEE Joint Propulsion Conference & Exhibit, San Diego, CA, 2011.
[25] Y. Aly, M. Schoenitz, E.L. Dreizin, Combust. Sci. Technol. 183 (2011) 1107–1132.
[26] S. Zhang, M. Schoenitz, E.L. Dreizin, Metastable aluminum-based reactive composite materials prepared by cryomilling, in: 50th AIAA Aerospace Sciences Meeting, Nashville, TN, 2012.
[27] S. Zhang, C. Badiola, M. Schoenitz, E.L. Dreizin, Combust. Flame 159 (2012) 1980–1986.
[28] L.E. Fried, W.M. Howard, P.C. Souers, P.A. Vitello, Cheetah 6.0 User Manual, Report No. LLNL-SM-416166, Lawrence Livermore National Laboratory, 2010.
[29] C. Suryanarayana, Prog. Mater Sci. 46 (2001) 1–184.
[30] R. Jeenu, K. Pinumalla, D. Deepak, J. Propul. Power 26 (2010) 715–723.
[31] O.G. Glotov, V.Y. Zyryanov, Combust. Explos. Shock 31 (1995) 72–78.
[32] R.L. Geisler, A global view of the use of aluminum fuel in solid rocket motors, in: 38th AIAA/ASME/SAE/ASEE Joint Propulsion Conference & Exhibit, Indianapolis, 2002.
[33] E.W. Price, in: K.K. Kuo, M. Summerfield (Eds.), Fundamentals of Solid-Propellant Combustion, American Institute of Aeronautics and Astronautics, 1984, pp. 479–513.
[34] M.A. Trunov, M. Schoenitz, E.L. Dreizin, Combust. Theory Model. 10 (2006) 603–623.
[35] P.F. Pokhil, A.F. Belyayev, Y.V. Frolov, V.S. Logachev, Combustion of Powdered Metals In Active Media, Report No. FTD-MT-24-551-73, Air Force Systems Command, 1973.
[36] J.K. Sambamurthi, E.W. Price, R.K. Sigman, AIAA J. 22 (1984) 1132–1138.
[37] L. Meda, G. Marra, L. Galfetti, S. Inchingalo, F. Severini, L.T. DeLuca, Combust. Sci. Technol. 65 (2005) 769–773.
[38] R.J. Gill, C. Badiola, E.L. Dreizin, Combust. Flame 157 (2010) 2015–2023.
[39] C. Badiola, R.J. Gill, E.L. Dreizin, Combust. Flame 158 (2011) 2064–2070.
[40] C. Badiola, E.L. Dreizin, Combust. Sci. Technol. 184 (2012) 1993–2007.
[41] P. Lynch, H. Krier, N. Glumac, Proc. Combust. Inst. 32 (2009) 1887–1893.
[42] T.R. Sippel, Characterization of Nanoscale Aluminum and Ice Solid Propellants, Purdue University, West Lafayette, IN, MS Thesis, 2009.